Eur. Phys. J. D **34**, 315–319 (2005)
DOI: 10.1140/epjd/e2005-00166-9

THE EUROPEAN PHYSICAL JOURNAL D

Structures and reactions of hydrated biomolecular cluster ions

S. Nonose[1,a], S. Iwaoka[2], K. Mori[2], Y. Shibata[2], and K. Fuke[2]

[1] Faculty of Science, Yokohama City University, Yokohama 236-0027, Japan
[2] Department of Chemistry, Faculty of Science, Kobe University, Kobe 657-8501, Japan

Received 6 September 2004
Published online 13 July 2005 – © EDP Sciences, Società Italiana di Fisica, Springer-Verlag 2005

Abstract. Photo-induced reactions and metastable decompositions of cluster ions containing glycine, tryptophan, tryptophanylglicine and [Fe(III)-protoporphyrin]$^+$ (hemin$^+$) ions solvated with water molecules are studied with electrospray ionization (ESI). The ESI ion source is improved to produce hydrated biomolecular cluster ions. Metastable decompositions of the hydrated clusters following primary mass selection are measured to determine the incremental solvent binding energies for the clusters by using evaporative ensemble model. From these experimental findings, stability of the cluster ions is discussed in terms of delocalization of ionic charges. We also measure the photodissociation yields of mass-selected water clusters containing hemin$^+$ ions at 355 and 532 nm. The mass spectra of photofragments show the β-cleavage of carboxymethyl groups in addition to the evaporation of solvent molecules.

PACS. 36.40.-c Atomic and molecular clusters – 73.22.-f Electronic structure of nanoscale materials: clusters, nanoparticles, nanotubes, and nanocrystals

1 Introduction

The characteristic properties of water molecules lead to strong preference of water to interact with functional groups of biomolecules. As a consequence of strong water — solute interaction in the aqueous environment has a significant influence on the solute charge distribution. As shape and charge distribution are intimately related to biological activity of biomolecules, the solvent water is an integral part of a functioning biological system. NMR and X-ray diffraction methods have addressed the issue of hydration of biopolymers in condensed phases [1,2]. However, little microscopic information has been obtained from these methods about the contribution of the water molecules to the system stabilities. Gas-phase spectroscopic methods along with theoretical calculations provide detailed information on molecular structures of biomolecules [3,4]. However, these methods are limited to smaller model systems with typically one or two water molecules attached. Certain important processes that occur during stepwise hydration such as changes in the charge distribution are not explained by these simple modeling systems. In order to investigate the influence of an individual water molecule on the contribution of solvation to the system stabilities, the biomolecules with solvent waters should be introduced into vacuum as clusters. The gas phase is an unusual environment for the investigation of these biological molecules. However, the gas-phase studies are expected to provide a deeper understanding of hydration interactions that determine the structures and reactions. Therefore, investigations of clusters are expected to bridge the gap between the gas-phase reactions and the biological activities on condensed phase. Structures and reactions of gas-phase clusters have been studied extensively using various spectroscopic methods [5–9]. Recent advances in electrospray ionization (ESI) allow us to produce various kinds of nonvolatile molecules in the gas phase without destruction [10]. Fenn and coworkers have developed the method to produce hydrated cluster ions by using ESI [11,12]. Several groups have applied ESI to mass spectrometric studies of the gas-phase cluster ions [13–21]. In the present study, water clusters containing biomolecules such as glycine (Gly), tryptophan (Trp), tryptophanylglicine (TrpGly) and [Fe(III)-protoporphyrin]$^+$ (hemin$^+$) ions are produced by using ESI method. We measure metastable decomposition yields of the clusters to estimate incremental binding energies of solvent waters. We also investigate photo-induced reactions of water clusters containing hemin$^+$ ions in order to clarify the mechanism of the β-cleavage reaction. Because of characteristic properties of water, extensive solvation effects are observed for the reactions of water clusters containing biomolecular ions.

2 Experimental

Figure 1 shows a schematic diagram of the apparatus consisting of an ESI source and a tandem mass spectrometer with octapole ion beam guides. Ions of amino acids and peptides are produced by ESI of a dilute solution

[a] e-mail: nonose@yokohama-cu.ac.jp

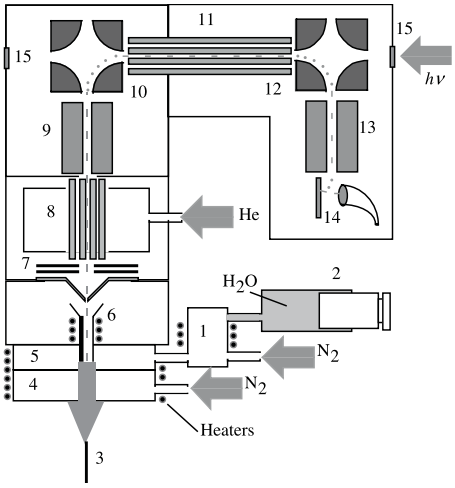

Fig. 1. Schematic diagram of the tandem mass spectrometer with ESI source; (1) vaporizing chamber, (2) syringe pump, (3) electrospray needle, (4) drying chamber, (5) solvation chamber, (6) stainless steel capillary, (7) skimmer and electrostatic lenses, (8) first octapole ion-beam guide with gas cell, (9) first quadrupole mass filter, (10) first quadrupole ion deflector, (11) second octapole ion beam guide, (12) second quadrupole ion deflector, (13) second quadrupole mass filter, (14) channeltron with conversion dynode, (15) quartz window.

of amino acids and a peptide, Gly, Trp and TrpGly (Sigma-Aldrich), in methanol including acetic acid (1.0%). $Hemin^+$ ions are produced by ESI of a dilute solution of Fe(III)-protoporphyrin chloride (hemin chloride, Wako Chemicals) in methanol-dichloromethane (1:1 v/v) mixture. Optimum intensity and stability of ion signals are obtained with a 5×10^{-4} M solution of the samples, which is delivered to the needle tip at a rate of 0.01 mL/min. The electrospray needle (3) is biased at 4.5−5.0 kV with respect to the drying chamber (4). The contemplated experiments require a continuous flow of bath gas; the mixture of inert carrier and solvent vapor with which the ions are to be solvated under well-defined conditions [11,12]. Temperature and composition must be independently variable over a wide range. Carrier gas from a high pressure source (nitrogen in these experiments) throttled by a stop valve passes via a mass flow meter (Brooks, 5850TR) through heated vaporizing chamber (1) into which solvating species (water in these experiments) are injected in liquid form at a desired rate by syringe pump (2). The resulting bath gas (carrier gas plus adduct vapor) enters the solvation chamber (5) at a rate such that the pressure in (5) is slightly above that in the drying chamber (4). All parts of the system downstream of (1) are heated so that the temperature of the bath gas (carrier gas plus water vapor) is always well above 350 K. An electric field between the injection needle (3) and the drying chamber (4) disperses sample solution into charged droplets that are driven by the field to the entrance of the chamber (4) which are an orifice 7 mm in diameter. A 0.5 L/min flow of heated drying gas (nitrogen) enters the chamber (4) through mass flow meter (Brooks, 5850TR) and it emerges from the entrance orifice countercurrent to the ions and charged droplets.

Ions from evaporating droplets are driven through the entrance of (4) and the partition orifice of (5) are admitted into the first vacuum chamber through stainless capillary (6). The first vacuum chamber is evacuated by a 290 m^3/h roots pump (ULVAC, YM-VD-300C). The ion beam is then passing through a stainless-steel skimmer (7), and is focused by electrostatic lenses into the first octapole-ion-beam guide (OPIG1) (8), which is equipped with a gas cell, in the second vacuum chamber. The second vacuum chamber is evacuated by a 2000 L/s diffusion pump (Edwards, Diffstak 250/2000C). The OPIG1 is connected directly to the first quadrupole mass spectrometer (QMASS1; ABB EXTEL, 664901) (9) in the third vacuum chamber evacuated by a 2000 L/s diffusion pump (Edwards, Diffstak 250/2000C). The mass-selected ions emerging from the QMASS1 are deflected 90° by a first quadrupole ion deflector (QDF1) (10), and are admitted into the second octapole-ion-beam guide (OPIG2) (11). High transmission efficiency for slow ions is accomplished by applying a radio frequency (RF) field to the OPIGs. The OPIG2 in the fourth vacuum chamber is jointed to the first and second quadrupole ion deflectors. The fourth chamber is evacuated with a 400 L/s turbo molecular pump (SEIKO SEIKI, STP-400). The difference of dc voltages between the skimmer and the OPIG2 corresponds to the kinetic energy of ions passing through OPIG2. After passing through OPIG2, the parent and product ions are deflected 90° by the second quadrupole ion deflector (QDF2) (12), and are admitted into the second quadrupole mass spectrometer (QMASS2) (ABB EXTEL, 652601) (13). The ions are detected by a channeltron electron multiplier equipped with a conversion dynode (14). By adjusting dc voltages of OPIG2 and QDF2, the collection efficiency of product ions having a sizable kinetic energy spread is maximized. Signals from the detector are fed into a preamplifier (Stanford Research Systems SR445). Single ion pulses are subsequently scored by a two-channel gated photon counter (Stanford Research Systems SR400), which is synchronized with the laser beam. Data acquisition and instrument control are managed by a personal computer through GPIB interfaces. Mass spectra showing the distribution of ions produced with ESI are obtained by switching off the DC voltage of QMASS1 and scanning QMASS2.

Mass spectra of photofragments are recorded by measuring production yields of the fragment ions. The laser beam is introduced into OPIG2 collinearly and counterpropergatedly with the ion beam. We use the 2nd or the 3rd harmonic of a YAG laser as light sources of the photolysis. In order to improve the intensities of the photodissociation spectra, the parent ions are trapped in OPIG1 (8). The gas cell is filled with helium and kinetic energies of the parent ions are reduced by multiple collisions with helium atoms. By getting up DC voltage of OPIG1, the trapped ions are extracted from OPIG1 to synchronize with the photolysis laser. Typical pulse width of the ions is 0.5 ms. Intensities of the photodissociation spectra are

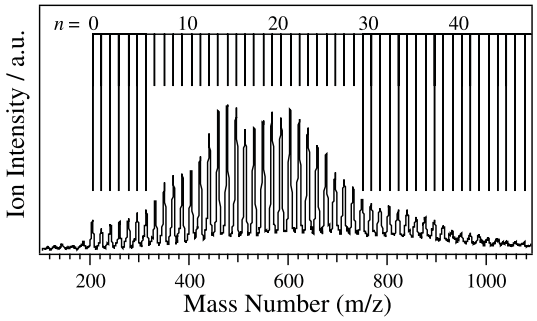

Fig. 2. Mass spectrum of hydrated tryptophan ion, $TrpH^+(H_2O)_n$.

improved by more than 30 times by using the pulsed ion beams. Laser fluence is attenuated to less than 3 mJ cm^{-2} to avoid multiphoton absorption. We carefully measure laser fluence dependence of photodepletion for the parent ions in 1−10 mJ cm^{-2}, and check that the distribution of product ions do not depend on the laser fluence.

3 Results and discussion

Typical mass spectrum of protonated tryptophan ions solvated with water molecules, $TrpH^+(H_2O)_n$, produced by ESI is presented in Figure 2 as a function of mass number, m/z. The observed mass spectrum consists of the hydrated cluster ions ranging from $n = 0$ to 40. Intensity and mass distribution of the ionic species produced by ESI depend strongly on the vapor pressure of water in the solvation chamber (5). High vapor pressure of water enhances production of large hydrated clusters. By optimization of the flow rate for the syringe pump (2), ions of specific cluster sizes are produced efficiently.

3.1 Incremental binding energies of hydrated amino acids and peptides ions

In order to examine the solvation energies of protonated amino acids and dipeptide ions, Gly, Trp and TrpGly, solvated with water molecules, we measure the metastable decomposition of the hydrated clusters. These clusters may proceed to sequential dissociation processes between initial mass selection and final detection. In Figure 3a, the metastable decay fractions of $GlyH^+(H_2O)_n$, $TrpH^+(H_2O)_n$ and $TrpGlyH^+(H_2O)_n$ by loss of one H_2O molecule are plotted as a function of cluster size. The metastable decomposition including the loss of two solvent molecules is not observed in the present experiment. The results indicate that the increase in the metastable fractions with increasing the cluster size is a characteristic of the evaporative ensembles. For $GlyH^+(H_2O)_n$, decay fraction is relatively small from $n = 1$ to 5, while those for $TrpH^+(H_2O)_n$ and $TrpGlyH^+(H_2O)_n$ are not so small. Incremental binding energies of H_2O for the hydrated clusters are estimated by using an evaporative

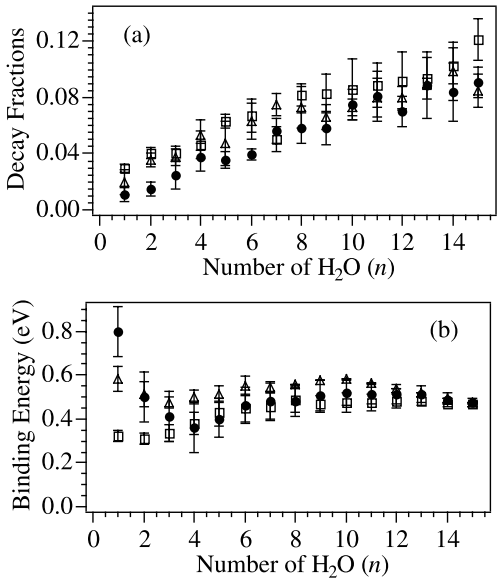

Fig. 3. (a) Decay fractions for the metastable decomposition of $GlyH^+(H_2O)_n$, $TrpH^+(H_2O)_n$ and $TrpGlyH^+(H_2O)_n$ are presented as filled circles, empty squares and empty triangles, respectively. (b) Incremental binding energies of H_2O molecule for $GlyH^+(H_2O)_n$, $Trp^+(H_2O)_n$ and $TrpGly^+(H_2O)_n$ are presented as filled circles, empty squares and empty triangles, respectively.

ensemble model. Details of the scheme for the estimation used in the present study have been described elsewhere [9,15,20]. Briefly, it is assumed that the evaporation occurs by a sequential loss of neutral monomers and at least one molecule evaporates before the detection. The kinetic energy release accompanying with metastable decay is also assumed to be twice as large as the available energy per one active vibrational degree of freedom. According to the classical RRK theory, rate constants of the unimolecular dissociation for the cluster ions are calculated. Iterative evaluations are performed until agreement is reached between the calculated and observed fractions for metastable decay. In order to estimate the absolute values of the incremental binding energies, those at $n = 16$ are assumed to be equal to the bulk enthalpy of vaporization of H_2O (0.456 eV). With this assumption, the binding energies are calculated. They are shown in Figure 3b. For $GlyH^+(H_2O)_n$, the binding energy decreases with increase of n from $n = 1$ to 4, whereas it increases gradually from $n = 5$. Kebarle and co-workers have determined the incremental binding energies of $GlyH^+(H_2O)_n$ clusters to be 0.73, 0.62, and 0.54 eV for $n = 1$−3, respectively, by using high-pressure mass spectrometry [14]. The present results qualitatively agree with them. For $TrpH^+(H_2O)_n$, the binding energy at $n = 1, 2$ is smaller than that for $GlyH^+(H_2O)_n$. It increases gradually with increase of n. Many groups have studied the site of protonation in $TrpH^+$. It has been reported that the proton is attached to the amino group, and that the protonated amino group is stabilized to interact with conjugated π-system of the indole group [19]. Therefore, the ionic charge would be

delocalized in $TrpH^+$. The ionic charge strengthens the hydrogen bond. Strength of the hydrogen bond depends on charge distribution in the ionic species. Because the ionic charge in $TrpH^+$ is more delocalized than that in $GlyH^+$, the binding energy of $TrpH^+(H_2O)_n$ at $n = 1, 2$ is much smaller than that for $GlyH^+(H_2O)_n$. As seen in the figure, the binding energy of $TrpGlyH^+(H_2O)_n$ is slightly larger than that of $TrpH^+(H_2O)_n$ at any n. Charge delocalization would be not so efficient for $TrpGlyH^+$, comparing with $TrpH^+$. Hydrations of hydrophilic amino acids such as histidine and arginine have also been studied [23]. Their results are similar to that for $TrpH^+(H_2O)_n$. Bowers group has determined binding energies of hydrated peptide ions, and analogous feature to the present work has been obtained [13].

3.2 Incremental binding energies of solvated Hemin$^+$ ions

We examine the metastable decomposition of water cluster ions containing hemin$^+$ and hemin$^+$-histidine complex (hemin$^+$His). Histidine is a typical ligand to heme in proteins, which control functions of heme. For comparison, hemin$^+$(pyridine)$_n$ is also examined. Hemin$^+$His ions are produced by ESI of a mixed dilute solution of hemin (Wako Chemicals) and histidine (Wako Chemicals) in methanol-dichloromethane (1:1 v/v) mixture. Optimum intensity and stability of ion signals are obtained with a solution of 5×10^{-4} M for hemin and 5×10^{-3} M for histidine. These clusters proceed to sequential solvent release between the initial mass selection and final detection. For hemin$^+$His$(H_2O)_n$, no histidine release is observed. Therefore, histidine would be tightly bound to the Fe atom of hemin with its imidazole group. Decay fractions for the metastable decomposition by loss of one solvent molecule of hemin$^+(H_2O)_n$, hemin$^+$His$(H_2O)_n$ and hemin$^+$(pyridine)$_n$ are presented in Figure 4a. For hemin$^+(H_2O)_n$ and hemin$^+$His$(H_2O)_n$, the decay fractions are relatively large at $n = 1$, and they increase gradually with increase of n. In contrast to that, for hemin$^+$(pyridine)$_n$, the decay fractions are small at $n = 1$, and they increase suddenly with increase of n. Incremental binding energies of solvent molecules for the clusters are estimated by using an evaporative ensemble model, which are shown in Figure 4b. For hemin$^+(H_2O)_n$ and hemin$^+$His$(H_2O)_n$, the binding energies at $n = 1$ are much small, they increase with increase of n, and there are the broad maximum at $n \backsimeq 10$, whereas that for hemin$^+$(pyridine)$_n$ is large at $n = 1$, and it decreases suddenly with increase of n. The binding energy of hemin$^+$His$(H_2O)_n$ is a little smaller than that of hemin$^+(H_2O)_n$ at any n. The water molecules are bound loosely to hemin$^+$ by electrostatic interaction, because the ionic charge in hemin$^+$ is extensively delocalized over conjugated π-system. The ionic charge in hemin$^+$His is still more delocalized than that in hemin$^+(H_2O)_n$. It is diffused into conjugated π-system of histidine. With increase of n, solvent waters are aggregated and number of hydrogen bonds for each

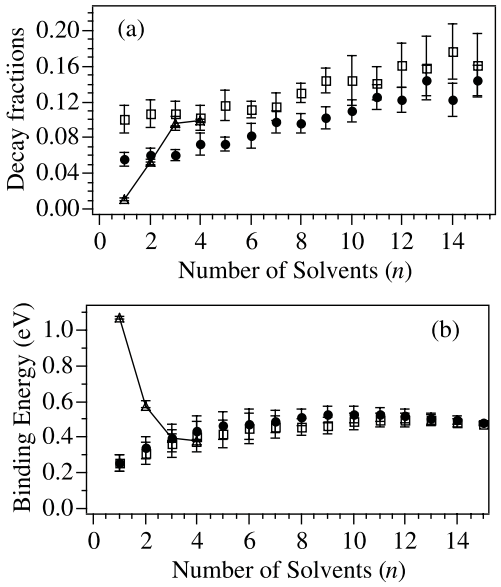

Fig. 4. (a) Decay fractions for the metastable decomposition of hemin$^+(H_2O)_n$ and hemin$^+$His$(H_2O)_n$ by loss of one H_2O are presented as filled circles and empty squares, respectively. That of hemin$^+$(pyridine)$_n$ by loss of one pyridine is shown as empty triangles with lines. (b) Incremental binding energies of H_2O for hemin$^+(H_2O)_n$ and hemin$^+$His$(H_2O)_n$ are presented as filled circles and empty squares, respectively. That of pyridine for hemin$^+$(pyridine)$_n$ is shown as empty triangles with lines.

molecules increases. Therefore, the binding energy increases gradually with increase of n from $n = 1$ to 10. Analogously, binding energy of $H_3O^+(H_2O)_n$ increases gradually with increase of n from $n = 9$ to 16 [22]. Similar result to that for hemin$^+$His$(H_2O)_n$ is obtained for hydrated clusters of hemin$^+$-1,4-diazabicyclo[2,2,2]octane (DABCO) [23]. DABCO is a typical electron donor and would be tightly bound to the Fe atom of hemin. The ionic charge in hemin$^+$DABCO would be also diffused into DABCO.

Incremental binding energy of hemin$^+$(pyridine)$_n$ are also estimated. Those at $n = 5$ are assumed to be equal to the bulk enthalpy of vaporization of pyridine (0.364 eV). Pyridine is a typical ligand to a transition metal. The first and second pyridines attached to the Fe atom by coordination bonds, while the third one is bound loosely by electrostatic interaction. In contrast to that for hemin$^+(H_2O)_n$, the binding energy is large at $n = 1$, 2 and they decrease suddenly with increase of n.

3.3 Photodissociation of Hemin$^+(H_2O)_n$ clusters

Figure 5 shows the mass distributions of the fragment ions produced by the photolysis of hemin$^+(H_2O)_n$ ($n = 0$–5) clusters with the 2nd (18 800 cm^{-1}) and the 3rd harmonic (28 200 cm^{-1}) of the YAG laser. Similar results are obtained for the photolysis of hemin$^+(CH_3OH)_n$ ($n = 0$–5) clusters [23]. In porphyrins, highest-occupied molecular orbital (HOMO) and lowest-unoccupied molecular orbital

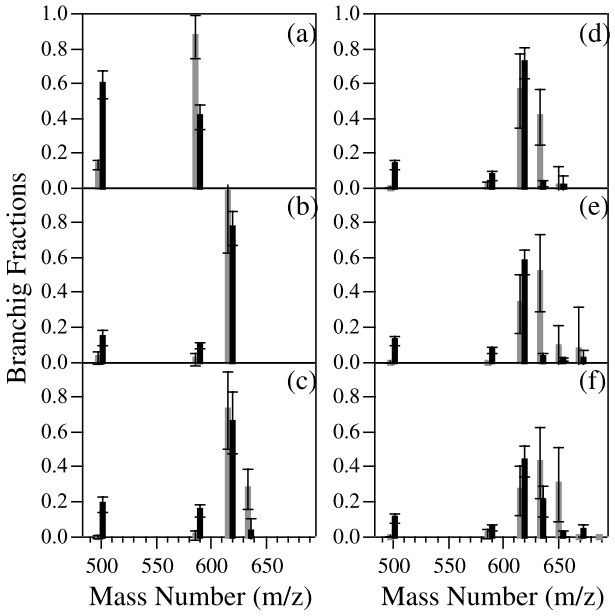

Fig. 5. Branching fractions of photofragment ions produced from hemin$^+$($H_2O)_n$ ($n = 0$ (a) to 5 (f)). The gray and black bars show the photoproducts generated with 2nd (18 800 cm^{-1}) and 3rd harmonic (28 200 cm^{-1}) of YAG laser, respectively.

(LUMO) are π–type orbitals. The irradiations at 18 800 and 28 200 cm^{-1} correspond to the excitations of $\pi\pi^*$ electronic states, which are ascribed to the $1E_u$ and $2E_u$ states, respectively [24]. As shown in the figure, the fragment ions generated through the decomposition of hemin$^+$ (617 amu) are observed at 558 and 499 amu in addition to the evaporation products such as hemin$^+(H_2O)_m$ ($0 \leq m < n$). The product ions at 558 and 499 amu are assigned to the fragments, which loss one and/or two carboxymethyl groups, –CH_2COOH (59 amu), by the β-cleavage of hemin$^+$, respectively. As seen in the figures, with increasing the excitation energy from 18 800 to 28 200 cm^{-1}, the evaporations of H_2O and the β-cleavage are enhanced for all n. Since we observe no indication of the reaction via an excited-state channel, the product ions are generated through the higher vibrational levels in the ground state repopulated via a fast internal conversion as follows; photoexcitation and repopulation of the higher vibrational levels of hemin$^+$ cluster ions in the ground state, subsequent sequential evaporation, and decomposition of hemin$^+$. In the present study, solvated product ions such as [hemin$^+ - k(CH_2COOH)](H_2O)_m$ ($k = 1$ or 2, $m \leq n$) are not observed. This result seems to indicate that both the evaporation and β-cleavage reaction may take place competitively. As seen in the figures, the decomposition of hemin$^+$ at 18 800 cm^{-1} is efficiently suppressed by the addition of a few solvent molecules. The branching fractions of β-cleavage in the photodissociation at 28 200 cm^{-1} are also affected by the solvation. However, the effect of solvation is rather small comparing with that for the 18 800 cm^{-1} excitation.

This work is partially supported by the Grant-in-Aid (Grants #11304042) from the Ministry of Education, Science, Sports and Culture of Japan, and by the Grant-in-Aid for Scientific Research (Grants #11740326, and #13640512) and a research grant for the future program from Japan Society for Promotion of Science.

References

1. P.S. Belton, Cell. Mol. Life Sci. **57**, 993 (2000), and references cited therein
2. M. Nakasako, Cell. Mol. Biol. **47**, 767 (2001), and references cited therein
3. E.G. Robinson, J.P. Simons, Phys. Chem. Chem. Phys. **3**, 1 (2001), and references cited therein
4. B.C. Bian, A. Longarte, T.S. Zwier, Science **296**, 2369 (2002)
5. *Clusters of Atoms and Molecules*, edited by H. Haberland (Springer-Verlag, Heidelberg, 1994), Vol. I and II and references cited therein
6. K. Fuke, K. Hashimoto, S. Iwata, Adv. Chem. Phys. **110**, 431 (1999), and references cited therein
7. S. Nonose, T. Taguchi, F. Chen, S. Iwata, K. Fuke, J. Phys. Chem. A **106**, 5242 (2002)
8. P. Brockhaus, I.V. Hertel, C.P. Schulz, J. Chem. Phys. **110**, 393 (1999)
9. J.A. Draves, Z. Luthey-Schulten, W.-L. Liu, J.M. Lisy, J. Chem. Phys. **93**, 4589 (1990)
10. *Electrospray Ionization Mass Spectrometry*, edited by R.B. Cole (Wiley, New York, 1997), and references cited therein
11. D.L. Zhan, J. Rosell, J.B. Fenn, J. Am. Soc. Mass Spectrom. **9**, 1241 (1998)
12. D.L. Zhan, J.B. Fenn, Int. J. Mass Spectrom. **219**, 1 (2002)
13. D. Liu, T. Wyttenbach, P.E. Barran, M.T. Bowers, J. Am. Chem. Soc. **125**, 9458 (2003)
14. J.S. Klassen, A.T. Blades, P. Kebarle, J. Phys. Chem. **99**, 15509 (1995)
15. T.G. Spence, T.D. Burns, G.B. Guckenberger, L.A. Posey, J. Phys. Chem. **101**, 1081 (1997)
16. X.-B. Wang, L.-S. Wang, J. Chem. Phys. **111**, 4497 (1999)
17. S. Rodriguez-Cruz, J.S. Klassen, E.R. Williams, J. Am. Soc. Mass Spectrm. **8**, 565 (1997)
18. M.F. Jarrold, Acc. Chem. Res. **32**, 360 (1999)
19. H. Lioe, R.A.J. O'Hair, G.E. Reid, J. Am. Soc. Mass Spectrom. **15**, 65 (2004)
20. S. Nonose, S. Iwaoka, H. Tanaka, N. Okai, T. Shibakusa, K. Fuke, Eur. Phys. J. D **24**, 335 (2003)
21. S. Nonose, H. Tanaka, N. Okai, T. Shibakusa, K. Fuke, Eur. Phys. J. D **20**, 619 (2002)
22. Z. Shi, J.V. Ford, S. Wei, A.W. Castleman, J. Chem. Phys. **99**, 8009 (1993)
23. S. Nonose, S. Iwaoka, H. Tanaka, T. Shibakusa, K. Mori, K. Fuke, unpublished results
24. M. Gouterman, J. Mol. Spectroscopy **6**, 138 (1961)